Modeling of Reinforced and Fiber-Reinforced Concrete Slabs under Impact Loads

Trevor D. Hrynyk and Frank J. Vecchio

SYNOPSIS: Current modeling procedures used to investigate the performance of reinforced concrete structures under impact are almost entirely confined to hydrocode approaches (e.g., LS-DYNA). While such procedures are capable of providing highly detailed representations of reinforced concrete structures and elements, they have often met with limited success due to the fact that: i) they typically employ complex micro-modeling representations of the structure under consideration, which can be expensive in preparation and computation, ii) they often require extensive characterization of material properties which are typically unknown, or calibration against previous test data, and iii) many of the commercial programs have shown deficiencies in their abilities to adequately capture cracked concrete response, particularly with regard to brittle shear-governed behavior.

This paper summarizes the application of an alternative modeling procedure for reinforced concrete slab and shell structures subjected to blast and impact loads. The nonlinear finite element program employed uses a layered thick-shell element with reinforced concrete constitutive modeling done in accordance with the formulations of the Disturbed Stress Field Model (DSFM), a smeared rotating crack procedure shown to be capable of accurately capturing the behavior of shear-critical elements under conventional static loading conditions. This approach differs from that typically used within hydrocodes and results in comparatively simple model construction and reduced computation costs. The program is used to model the response of intermediate-scale reinforced concrete and steel fiber-reinforced concrete (SFRC) slab-like elements tested under repeated high-mass low-velocity impacts. Using simple finite element meshing techniques and predefined material behavioral models requiring only basic user input, good correlation between the observed and modeled slab response was attained.

Keywords: reinforced concrete; impact; FRC; punching shear; nonlinear analysis; thick-shell; finite element.

ACI member **Trevor D. Hrynyk** is an Assistant Professor in the Department of Civil, Architectural and Environmental Engineering at the University of Texas at Austin. He is a member of Joint ACI-ASCE Committees 421, Design of Reinforced Concrete Slabs; 447, Finite Element Analysis of Reinforced Concrete Structures, and ACI Subcommittee 445-C, Punching Shear. His research interests include performance assessment and analysis of reinforced concrete structures, response under extreme loads, and reinforced concrete slabs and shells.

Frank J. Vecchio, FACI, is a Professor in the Department of Civil Engineering at the University of Toronto. He is a member of Joint ACI-ASCE Committees 441, Reinforced Concrete Columns; 447, Finite Element Analysis of Reinforced Concrete Structures. He received the 1998 ACI Structural Research Award, the 1999 ACI Structural Engineer Award, the 2011 ACI Wason Medal for Most Meritorious Paper, and the 2016 Joe W. Kelly Award. His research interests include advanced constitutive modeling and analysis of reinforced concrete, assessment and rehabilitation of structures, and response under extreme loads.

INTRODUCTION

Designing reinforced concrete (RC) structures to withstand blast and impact loads has traditionally been approached in a highly idealized manner, with procedures typically consisting of empirical formulas used to estimate member damage levels or capacity (Sliter 1980; Kishi et al. 2002) and macro-modeling procedures that reduce structural members to limited or even single-degrees-of-freedom (UFC 3-340-02 2008). Although the simplicities of such methods make them highly appealing and often practical, they have been shown to be unreliable in some cases (El-Dakhakni et al. 2009; Chen and May 2009) and they generally provide limited information regarding the actual dynamic response and post-event state of the structure. As modern code provisions continue to evolve toward performance-based design methodologies, and as extreme loading scenarios such as impact and blast are considered in the design process more regularly, the need for analytical tools which are capable of accurately modeling the behaviors of complex RC structures under a wide range of loading conditions continues to grow.

Several commercial programs have been developed to analyze RC elements and infrastructure under general loading conditions, including blast and impact. However, these tools are almost entirely confined to hydrocode procedures such as LS-DYNA, and often such approaches have met with limited success as they typically require complex micro-modeling representations of the structure or element under consideration which is expensive in model preparation and computation, and many of the available commercial programs have shown deficiencies in their abilities to capture the responses of shear-critical elements. Some researchers have suggested that further analytical advancement in the areas of blast and impact has been hindered by a lack of high-quality experimental data (Chen and May 2009). As such, the development of alternative analytical tools which are practical, employ rational modeling approaches capable of capturing the behavior of shear-critical elements, and are capable of analyzing RC structures under general loading conditions represents a research area which is both significant and relevant to the design of modern concrete infrastructure.

This paper presents the modeling approach and results from the nonlinear finite element analyses of RC and R/FRC (steel fiber-reinforced concrete containing conventional steel reinforcing bars) intermediate-scale slabs subjected to repeated high-mass low-velocity impact loading conditions. The finite element program used employs a layered ‘thick-shell’ formulation which rigorously accounts for out-of-plane (i.e., through-thickness) shearing effects. This feature, combined with the application of advanced behavioral modeling dedicated to the analysis of cracked RC and R/FRC, differs greatly from the computational procedures typically used to investigate RC structures under impact and is shown to provide high accuracy and adequate resolution computational estimates for the responses of the impact-loaded slabs, while maintaining simple model construction procedures and requiring limited computational effort.

ANALYSIS PROCEDURE BACKGROUND

The RC slab and shell structure analysis procedure presented in this work is implemented within the framework of a nonlinear finite element program employing layered thick-shell elements. The analysis program was originally developed by Figueiras and Owen (1984) in the 1980s for the analysis of conventional RC shells and slabs and, at that time, it had many noteworthy features. Perhaps of greatest significance, the RC shell structure analysis program

accounted for the development of through-thickness shear deformations using Mindlin theory (Mindlin 1951) and employed a nine-noded quadratic shell element that was shown to provide good performance in both thick- and thin-shell applications. In the early 1990s, the software program was modified by Polak and Vecchio (1993) through replacement of the governing behavioral models with that of the constitutive formulations of the Modified Compression Field Theory (MCFT) (Vecchio and Collins, 1986), a smeared fully-rotating crack procedure used to model the response of cracked RC elements under biaxial stress conditions. With the implementation of the MCFT, the program was shown to provide good response estimates for a broad range of RC slabs and shells under in-plane, out-of-plane, and combined in-plane and out-of-plane loading scenarios. More recently, several modifications have been made to the program to improve overall performance and to expand the range of applications that can be considered. This most recent set of modifications has included: i) the implementation of an alternative sectional analysis procedure used to account for through-thickness shearing effects in the layered elements (Hrynyk and Vecchio 2015), ii) cracked concrete material modeling in accordance with the formulations of the DSFM (Vecchio 2000), a hybrid rotating-fixed crack procedure developed as an extension of the formulations of the MCFT, iii) the addition of cyclic and dynamic analysis capabilities (Hrynyk 2013), and iv) element material modeling permitting the analyses of slabs and shells comprised of modern materials (e.g., fiber-reinforced concretes (FRC)) or constructed using alternative RC design techniques (e.g., steel-concrete (SC) composite construction) (Hrynyk and Vecchio 2016). It should be noted that these most recent program modifications (items i through iv above) play key roles in the RC and R/FRC slab impact analyses forming the focus of this paper.

The Layered Shell Element:

The layered finite element employed in the software is used to account for variations of material stress, strain, and stiffness through the thickness of the shells. Local stresses are assumed to be constant over the height of an individual layer and are integrated using sampling points located at the layer midheight. In-plane reinforcement can be defined in any planar orientation and is incorporated discretely within the thickness of the element (i.e., in-plane reinforcement is not smeared or distributed throughout the concrete layers). Transverse reinforcement oriented in the out-of-plane direction (i.e., in the local z-direction) is treated in a smeared sense, and is considered in the material modeling of the core concrete layers.

In its current state, the through-thickness response of the layered thick-shell element is based on the assumptions that i) plane sections remain plane, but not necessarily normal to the element midsurface, ii) out-of-plane normal stresses are negligible and, iii) according to the through-thickness formulation presented by Hrynyk and Vecchio (2015), the 'effective' out-of-plane shear strain distribution used to calculate cracked concrete material response can be approximated as being parabolic through the thickness of the shell element. Note that in this application the 'effective' out-of-plane shear strains represent only a part of the total shear strain, and may be comprised of net strains, plastic strains, elastic offset strains, and crack-slip strains. The layered element concept and typical through-thickness sectional response conditions, which illustrate assumptions i and iii noted above, are presented in Figure 1.

RC Constitutive Modeling:

Cracked concrete behavioral modeling is done on the basis of the formulations of the Disturbed Stress Field Model (DSFM) (Vecchio 2000). This smeared, hybrid rotating-fixed crack, analysis procedure inherently considers the redistribution of internal forces that can occur due to local changes in stiffness arising from cracking or crushing of concrete, yielding of the steel reinforcement, concrete compression softening attributed to the presence of lateral tension, the presence of post-cracking concrete tensile stresses between crack locations, and influences associated with variable and changing crack widths (including slip deformations along crack surfaces). Additional details regarding the implementation of the DSFM, which was originally developed to model the response of RC elements under biaxial stress conditions, in the context of the three-dimensional shell element analysis procedure forming the basis of the analyses summarized in this work, are provided elsewhere (Hrynyk and Vecchio 2015).

SLABS UNDER HIGH-MASS LOW-VELOCITY IMPACT

The data used to corroborate the impact analysis capabilities of the RC slab and shell structure software program are from a recent experimental investigation performed at the University of Toronto (Hrynyk and Vecchio 2014). Seven intermediate-scale slabs with uniform geometries were loaded under repeated high-mass low-velocity impact. The test slabs were 1,800-mm (71-in.) square, 130-mm (5.1-in.) thick, and were doubly-reinforced in both planar directions

such that four layers of longitudinal steel reinforcing bars were provided. Three of the seven slabs were constructed using a conventional concrete mixture design and the remaining four slabs were constructed using a steel fiber-reinforced concrete (SFRC) mixture design with fiber volume fractions ranging from 0.50 to 1.50 %. The longitudinal reinforcement ratios of the slabs ranged from 0.27 to 0.59 % in each planar direction (per layer of steel), and the steel fibers used in the R/FRC slabs (i.e., SFRC slabs containing conventional steel reinforcing bars) consisted of Dramix® RC-80/30-BP high strength end-hooked steel fibers. The cylindrical compressive strengths of the concrete comprising the slabs ranged from 45 to 69 MPa (6.5 to 10 ksi) and the maximum nominal aggregate size was 13 mm (0.50 in.). The typical geometries, reinforcement details, and estimated static load capacities for the slabs comprising the impact testing program are summarized in Figure 2. As shown in Figure 2c, all of the slabs comprising the testing program were designed such that under conventional center-point monotonic loading conditions, a ductile failure mode consisting of tension steel yielding would be epxpected to govern failure. Note that the flexural capacities of the RC slabs were estimated using yield-line theory (Johansen 1943) and their punching capacities were estimated on the basis of the provisions of ACI 318-14.

The slabs were restrained at their corners and impacted at their centers. Corner support assemblies restrained vertical translations but permitted spherical rotations and lateral slab expansions (i.e., planar expansions). The high-mass low-velocity impact loads were generated using a drop-weight testing method (see Figure 3). The drop-weight impactor consisted of a concrete filled square hollow structural steel section with mounting brackets that allowed impactor mass adjustments. The striking face of the drop-weight consisted of a 25-mm (1.0-in.) thick, 300-mm (11.8-in.) square steel plate that produced a flat hard-impact loading condition (Kennedy 1976). The weight was dropped from a constant height, producing a constant nominal impact velocity of 8.0 m/s (26.2 ft/s) which was verified using high-speed photography. A common loading protocol involving consecutive impacts of progressively increasing mass levels was used for all slabs. The impact mass level ranged from 150 to 300 kg (331 to 660 lb) and the number of impacts performed on each of the slabs ranged from 3 to 10 impacts. The slabs comprising the testing program were well-instrumented. Typically, twenty-five linear potentiometers were used to measure the transverse and lateral slab displacements. Thirteen accelerometers were used to measure transverse slab accelerations and to characterize the impact force generated by the drop-weight. Longitudinal reinforcing bars from each of the four layers of steel were instrumented with electrical-resistance strain gauges. High-strength rods forming the slab reaction frame were also instrumented with strain gauges to measure uplift (negative) reaction forces. Load cells were provided at each of the four corner supports to measure positive vertical reaction forces. Instrument measurements were collected using a digital data acquisition system and were acquired without filtering. Data collected from the accelerometers and the load cells were sampled at a rate of 96 kHz and data collected from the potentiometers and strain gauges were sampled at 2.4 kHz. Additional details pertaining to the positioning of the instrumentation and the test setup are available elsewhere (Hrynyk 2013).

For brevity, detailed numerical results from the analyses of only two of the seven slabs comprising the experimental program are presented in the following sections of this paper: RC slab TH2 and R/FRC slab TH4. These slabs were nominally identical in all aspects with the exception that R/FRC slab TH4 was constructed with a SFRC mixture containing a steel fiber volume fraction of 1.0 % (refer to Figure 2b). Both slabs contained conventional steel longitudinal reinforcement ratios of 0.42 % in each planar direction and, in contrast to their expected failure modes under conventional quasi-static loading conditions, both slabs were shown to be ultimately governed by punching shear failures under high-mass low-velocity impacts. RC slab TH2 was subjected to three impacts with mass levels ranging from 150 to 210 kg (331 to 463 lb) and R/FRC slab TH4 was subjected to seven impacts with mass levels ranging from 150 to 270 kg (331 to 595 lb). Note that for all other slabs comprising the testing program, an overview of the numerical results obtained, and discussion regarding the adequacy of those results in terms of estimating the experimentally measured responses, are provided.

MODELING APPROACH

The seven RC and R/FRC slabs comprising the experimental testing program were subjected to a total of 38 impact events and, for all cases, a common finite element mesh was used in the numerical modeling. A one-quarter slab finite element model was developed for the analyses of the impact-loaded slabs. Sixty-five layered shell elements and four out-of-plane truss bar elements were used to represent the quarter-slab specimens and the impacting drop-weight (see Figure 4). A total of 298 nodes comprised the slab mesh, resulting in a model with 1,295 total degrees of freedom. The shell elements forming the slab specimens were subdivided into 25 equal-thickness concrete layers, with an

additional four layers provided to represent the four layers of in-plane longitudinal steel present in each of the slabs. In the case of the R/FRC slabs, the end-hooked steel fibers were treated as a property of the concrete and, as such, were assumed to be uniformly distributed throughout the concrete layers of the shell elements.

To enforce symmetry, lateral and rotational restraints were provided along the slab centerlines forming the edges of the finite element model. The support reaction assemblies at the slab corners were incorporated through the vertical restraint of a single node within the quarter-slab mesh, located at the center-point of the test frame reaction assembly. Note that because the intent of the experimental program was to provide boundary conditions which both resulted in a stable support condition but also minimized the development of axial (i.e., lateral) confining stresses resulting from lateral support restraints, it was assumed that a simple roller restraint, that permitted rotations and translations in the plane of the slab, would be adequate in representing the restraint conditions provided in the testing program.

The near-rigid drop-weight was modeled using a single shell element with a large material stiffness assignment. To accommodate the flat striking face of the drop-weight used in the experimental program, the nodes comprising the rigid element were allowed to translate vertically in the global-z direction (i.e., the out-of-plane direction) and all rotations and in-plane translations were restrained. The drop-weight was connected to the shell elements forming the center-point impact region of the slab using four linear elastic 'compression-only' truss elements. The massless truss bar elements were also assigned large stiffness values (k_{truss} = 5x10^6 kN/mm (28.6x10^6 k/in.)), simulating the hard impact loading scenario used in the testing program. It is important to note that because the truss elements joining the drop-weight and the slab were only capable of developing compressive stresses, no uplift impact forces were generated as a result of mass rebounding.

As the layered shell finite elements employed rely on the assumptions that plane sections remain plane and out-of-plane confining effects are negligible, local disturbances stemming from concentrated loads or, in this case, an impacting mass, will typically not be captured well and, as a result, the 'thick-shell' finite element procedure has the tendency of underestimating the shear resistance of elements comprising disturbed regions. Thus, a form of out-of-plane shear strength enhancement similar to that employed by others (Bentz 2000; Guner 2008) was applied to the shell elements forming, and immediately surrounding, the impact regions of the slab (refer to Figure 4). To enhance the shear strength of the disturbed elements, the net out-of-plane shear strains computed within these elements were reduced by a factor of two, resulting in an apparent shear stiffness enhancement. In assigning this shear strength enhancement, it was assumed that the disturbed region extended over a distance equal to the effective reinforcement depth, *d,* away from the edges of the loaded area (i.e., from the edges of the mass impact region). Considering the reinforcement depths in the orthogonal directions, the average *d* value was taken as 100 mm (4 in.).

The loading for each impact event was simulated by specifying an initial velocity of 8.0 m/s (26.2 ft/s) to four lumped masses that were assigned to the mid-side nodes of the rigid drop-weight element. Note that because a one-quarter slab model was considered, the lumped masses assigned to the drop-weight totaled one-quarter of the actual impact mass used in the experiments. In addition to the initial velocity assignment, a constant mass acceleration of 9.81 m/s^2 (32.2 ft/s^2) was also specified to the drop-weight masses to simulate gravitational effects. Because the test slabs in the experimental program were subjected to sequential impact loading, it was necessary to perform a series of analyses for each test specimen, with each analysis representing a single impact event. Upon completion of each event analysis, numerically-generated data reflecting the damaged strain state and the slab's strain history were recorded in binary format that could then be used to resume the analysis, or analyze the damaged structure under alternative loading conditions. To minimize the required computation time to perform the full series of analyses, only the initial 200 milliseconds of each impact response-time history was computed. It was assumed that this event duration was long enough to assess the computed post-impact response characteristics of the slabs (i.e., damping behaviors and residual displacements) and that only minimal, if any, slab damage would occur as a result of the additional low amplitude response oscillations that were typically estimated, and experimentally observed, to occur at the ends of the 200 millisecond events. Additionally, it should be noted that, as a result of this technique, secondary impacts attributed to mass rebounding which occurred after the initial 200 milliseconds of the impact event were neglected.

Prior to performing the dynamic analyses on the damaged slabs, intermediate analyses were first required to return the drop-weight from its rebounding state back to its initial starting position. To do this, a monotonic analysis consisting of only one load stage with a 10 N (2.2 lb) point load was applied to the drop-weight. This small load level was enough to position the rebounding drop-weight in contact with the slab without causing any meaningful slab displacements. Additionally, the performance of the intermediate monotonic analysis was also used to reset all motion parameters (nodal velocities, nodal accelerations) from the end of the previous impact analysis, to values of zero.

Behavioral Models and Analysis Parameters:

While the material modeling of the RC shell elements is based principally on the formulations of the DSFM, several other behavioral models were also used to account for mechanisms that fall outside of the cracked concrete material model (e.g., concrete confinement and dilatation, incorporating influences associated with steel fibers, concrete and steel hysteretic responses, dowel action, strain rate effects, etc.). A summary of the material models and analysis parameters that have been used in the modeling of the reinforced concrete slabs under impact loads is summarized in Table 1. It should be noted that, with the exception of the steel hysteresis model, all of the material models used in the impact slab analyses were predefined 'default' materials that have been previously recommended for the analysis of RC slabs and shells under more conventional monotonic and cyclic loading conditions (Hrynyk 2013). In this case, the use of an alternative steel hysteresis model was selected to limit the amount of reinforcing bar plastic strain recovery attributed to the post impact low amplitude response cycling that was shown to occur in the slabs. Additional details regarding the selection of the steel hysteresis model are provided elsewhere (Hrynyk 2013). Further, it should also be noted that all of the material models used require only basic user input, consisting of parameters that are generally easy-to-define (e.g., f_c') Additional details regarding the supplementary material models and analysis parameters are provided elsewhere (Wong et al. 2013).

To capture the response of the SFRC material comprising the R/FRC slabs, the Simplified Diverse Embedment Model (SDEM) was employed (Lee et al. 2013). The SDEM is used to describe the tensile response of cracked concrete containing a random distribution of discontinuous steel fibers. Average fiber tensile stresses across cracks are computed as the summation of stresses developed from frictional bond and stresses developed from mechanical anchorage effects (e.g., due to fiber end-hooks). One of the main benefits of using the SDEM within the layered shell element procedure is that the application of the model requires only basic user input pertaining to fiber type, geometry, tensile strength, and volume fraction to estimate the SFRC material response. This feature is essential in keeping with the overall practical modeling procedure employed by the RC slab and shell structure analysis program. Details regarding the implementation of the SDEM within the DSFM-based cracked concrete modeling procedure are available elsewhere (Lee et al. 2016).

For all cases, the direct tensile strengths of the slabs were approximated as $0.33\sqrt{f_c'}$ in units of MPa ($4\sqrt{f_c'}$ in units of psi), the slab densities were taken as 2,400 kg/m^3 (150 lb/ft^3), and Popovics HSC model (Wong et al. 2013) was selected as the compression base curve for the 50 MPa (7.3 ksi) nominal strength concretes. The specified convergence tolerance was specified as 1.000050 and was computed on the basis of nodal displacements (translations and rotations). Solution under-relaxation was applied using a constant averaging factor of 0.50, which averaged the local strain values from one iteration to the next. Lastly, a maximum of 30 iterations were performed within each time step of the analyses.

Time Stepping Integration

The impact analyses of the test slabs were performed using Newmark's average acceleration method (Newmark 1959). Ideally, when using this time stepping procedure, a time step which is at least one order of magnitude smaller than the period of the highest contributing modal frequency should be selected. However, knowing in advance which modes contribute significantly to the overall response is nearly impossible, particularly in the case of nonlinear multi-degree-of-freedom systems. Thus, the selection of the time step used in the analyses of the slab impact tests was based on a limited investigation of the analytical response of impact event TH2-1 (i.e., the first impact test on RC Slab TH2). The analysis case of an initial impact event on an undamaged (i.e., high-stiffness) slab was chosen as it represents an analysis scenario which was likely to require the smallest time step size to achieve reasonable levels of accuracy. Analyses were performed using time steps ranging from 0.001 to 0.00001 s, and all other parameters were kept constant.

The computed midpoint displacement-time histories from five analyses performed using different time steps are presented in Figure 5. The use of the 0.001 s time step, which was the largest step size considered, produced an unstable response. Additionally, the displacement amplitude and the period of the midpoint displacement response computed using the large time step were significantly greater than those calculated using smaller step sizes. Results obtained using the 0.0005 s time step were stable throughout the analysis; however, differed significantly from those computed using smaller step sizes. Lastly, the results obtained using time steps ranging from 0.0001 to 0.00001 s exhibited higher levels of agreement amongst each other, with significantly less variation in period and displacement amplitude. Based upon these results, a time step of 0.0001 s was selected for the performance of all of the slab impact

analyses. The use of this time step for the analysis of impact event TH2-1 resulted in reasonable solution accuracy, achieving near perfect agreement in the initial phase of the response when compared to that obtained using smaller step sizes. Further, it should be reiterated that the investigation regarding time step requirements was performed considering an undamaged slab. Subsequent analyses considering impact events performed on damaged slabs with reduced stiffnesses were expected to result in improved numerical accuracy as a result of reduced frequency contents.

Supplemental Damping

For the purpose of enhancing solution stability, low levels of supplemental stiffness proportional damping were considered for all of the slab impact analyses performed. The use of stiffness proportional damping was selected as it ensured that as the stiffness of the slabs decreased due to the development of damage, the level of supplemental damping would also decrease. It must be emphasized that the actual damping of the computed slab impact responses are attributed to the steel reinforcement and cracked concrete material hystereses and not the inclusion of supplemental damping. In all cases, the level of proportional damping specified in the analysis resulted in damping ratios of less than 0.65 % of critical assigned to the first mode. Additional details regarding the implementation and the selection of the supplemental stiffness proportional damping are available elsewhere (Hrynyk 2013).

Strain Rate Effects

Dynamic increase factors (DIF) were used to account for material strain rate effects. The selection of the strain rate effect models was done on the basis of that used by others for similar DSFM-based analysis procedures (Guner and Vecchio 2012). The DIF-strain rate relationships used for concrete are based on the provisions of the *fib* Model Code 2010, and those for the steel reinforcing bars are in accordance with the model proposed by Malvar and Crawford (1998). To assess the influence of the dynamic increase factors on the computed responses of the impact-loaded slabs, analyses were performed with and without the inclusion of strain rate effects. In addition to the selected combination of concrete strain rate models, an alternative strain rate model for steel reinforcing bars based on the provisions of a CEB-FIP synthesis report (CEB-FIP 1988) was also examined.

Figure 6 presents numerical results computed using different material strain rate relations against those measured experimentally for impact event TH2-1. It can be seen that the analyses considering strain rate effects produced significantly stiffer responses. The peak center-point displacement, the period of the response, and the residual midpoint displacement were all reduced as a result of strain rate-based material enhancement. The support reactions, however, were only marginally affected by the inclusion of rate effects. The calculated peak reaction forces were nearly identical in all cases, and differences in the support reaction-time history response attributed to the inclusion of rate effects were essentially limited to the response period.

The computed response of the slab was found to be impacted greatly by the inclusion of strain rate effects, with the general tendency being that strain rate enhancement led to stiffer computed responses and reduced displacement amplitudes that showed better agreement with experimental data. Similar responses were computed using different strain rate models for the steel reinforcing bars suggesting that, for this specific analysis case, either of the two models considered would be suitable. However, the combination of the DIF-strain rate relations proposed by *fib* Model Code 2010 and the model for steel reinforcing bars proposed by Malvar and Crawford (1998) were used exclusively in all subsequent impact analyses presented in this paper.

RESULTS

This section provides details of the computed responses for RC slab TH2 and R/FRC slab TH4. Further, general findings regarding the suitability of the numerical estimates developed for impact loaded slabs, considering all impact events comprising the testing program, are summarized. For comparison purposes, the computed center-point displacement-time, total support reaction-time, and impulse-time histories have been plotted alongside the experimental results for each impact event. Additional discussions pertaining to the computed slab deformation behaviors and the reinforcing bar strain-time histories are provided for selected impact events.

RC Slab TH2: ($\rho_l = 0.420$ %; $V_f = 0$)

RC slab TH2 contained 0.42 % longitudinal reinforcement, per layer, in each planar direction and was constructed with conventional concrete. The slab was subjected to a total of three impact events, with drop-weights ranging from

150 kg (331 lb) to 210 kg (463 lb). Slab failure occurred under the third and final impact, and was experimentally found to be governed by punching shear.

Response-time histories from the analyses of the three impacts performed on RC slab TH2 are presented in Figure 7. From the displacement-time histories presented it is evident that the slab impact analyses accurately estimated the peak center-point displacements in all cases. Slab damage, in the form of residual center-point displacement, was not captured well in the analysis of the initial impact performed on the undamaged slab (i.e., impact event TH2-1). However, the analysis of subsequent impact events considering the already damaged slab provided good estimates of the displacement rebound amplitudes and of the residual displacements. Comparing the computed support reaction-time histories to those measured experimentally, it can be seen that the peak reaction forces were underestimated in the three impact events; however, the general shapes of the computed reaction-time responses seem to be in agreement with the experimental data. Examination of the calculated support reaction impulses shows that although the peak reaction values were underestimated in all cases, the computed impulses obtained from integrating the support reaction-time histories agree well with the experimental data and had the tendency to marginally overestimate the peak impulse within the first cycle of the response.

Displacement profiles from the three impacts performed on slab TH2 are presented in Figure 8. The displaced shapes shown represent the slab deformations at the time of the peak computed center-point displacement, and have been plotted against the peak experimental displacement profiles. It can be seen that the computed displacement profiles of slab TH2 are in good agreement with the experimental results. The shell element based analysis procedure estimated the initial development of localized deformations under the second impact as a result of punching, and in the analysis of the third impact event (event TH2-3), the punching-attributed failure of the slab was accurately captured. The slab displacements computed across the width of the slab section closely matched the experimental data in all three impact events. It should be noted that with regard to the measured peak displacement profile corresponding to the third impact, the experimental punching region was measured on the bottom surface of the slab. As such, the length of the punched region measured experimentally was found to be larger than that computed with respect to the mid-height of the slab.

Lastly, computed reinforcing bar strain-time histories for RC slab TH2 are compared alongside experimental strain measurements in Figure 9. Note that the computed strain results represent average reinforcing bar strain values as opposed to local reinforcement strains computed at crack locations. Strain gauge S1, which was located in the center-point region of the slab on the interior bottom-face mat of reinforcement, was considered. In general, it was found that that the accuracy of the computed bar strains was less consistent than that of the computed displacements or reactions and, in many cases, the estimated strains differed significantly from those measured experimentally. In the first two impact analyses pertaining to slab TH2, the calculated peak bar strains and the initial shape of the strain-time history response closely matched the experimental data (see Figure 9a and 9b). However, the post-peak responses were computed with less accuracy, with the general tendency being underestimations of the residual strains and overestimations of the response amplitudes. From Figure 9c, it can be seen that the analysis of the third and final impact of slab TH2 resulted in significant overestimation of both the peak strain level and the residual bar strains. Some variation amongst numerical and measured reinforcing bar strains is expected due to the localized nature of the strain measurements. However, in this case, it is believed that much of the disagreement observed between the computed and measured bar strains is attributed to the comparison of computed average steel strain values against local strain measurements.

R/FRC Slab TH4: ($\rho_l = 0.420$ %; $V_f = 1.0$ %)

R/FRC slab was nominally identical to slab TH2, with the exception that SFRC with a fiber volume fraction of 1.0 % was used in place of nonfibrous conventional concrete. A total of seven impact events were performed on slab TH4, with impact mass levels ranging from 150 kg (331 lb) to 270 kg (595 lb). Failure of the R/FRC slab was also governed by punching; however, the punching shear failure occurred in a more controlled manner, under significantly greater impact load, and was not accompanied by the extensive localized impact damage (e.g., mass penetration, concrete scabbing) that was shown to occur in the RC slabs.

The analyses of impact tests performed on R/FRC slab TH4 are plotted alongside the experimental responses in Figure 10. For brevity, results from only four of the seven impact events performed on TH4 are provided. Throughout the sequence of analyses performed, the computed responses remained stable and provided reasonable estimates of the experimental behaviors. Analyses of the first five impacts (events TH4-1 through TH4-5) resulted in high accuracy estimates of the center-point displacements and damping characteristics, and reasonable estimates of the response periods. The computed support reaction-time histories of the initial impacts agreed reasonably well with the

experimental responses, but reduced accuracies were attained over the progression of the sequential impact protocol. In all cases the peak reactions were underestimated; however, the amplitudes of the post-impact responses (i.e., after the first half-cycle) were computed well.

The analyses of the sixth and seventh impacts provided less accurate estimates of the experimental responses: the peak center-point displacements were slightly overestimated, the periods of the computed response periods were overestimated, and the general shapes of the support reaction responses showed little agreement with the high frequency responses measured experimentally. Further, the overall stiffness of slab TH4 was underestimated in the final impacts; however, most of the peak displacements were recovered resulting in underestimation of the residual displacements.

Overview of Computed Slab Response-Time Histories:

A summary of the computed and measured peak center-point displacements for all impact events performed on the RC and R/FRC slabs is provides in Table 2 and Table 3, respectively. In general, it can be seen that good agreement between the computed and the measured responses were obtained for the RC and R/FRC slabs comprising the experimental program. When the results from a total of 36 RC and R/FRC slab impact events are considered, the RC shell element analysis procedure was found to achieve a mean computed-to-experimental center-point displacement ratio of 1.06 with a coefficient of variation of approximately 13 %.

Comparison of the computed and measured center-point displacement results, also presented in Table 2 and Table 3, shows that, in general, lower accuracy estimates were obtained for residual displacements. The computation of the residual slab displacements poses a significant challenge as they rely heavily on accurate modeling of several complex behavioral mechanisms: localized material damage, post-peak material responses, and plastic strain development in the materials, all of which are difficult to estimate, even in specimens subjected to well-defined loading conditions. The current modeling procedure only considers steel plastic strain development from average reinforcing bar yielding. Plastic reinforcing bar strains developed across the crack locations are not retained, which is likely to also play a role in underestimating the residual slab displacement. Further, some consideration should be given to the magnitudes of the slabs' residual displacements, particularly those corresponding to the initial impacts. If the analytical estimates from all 36 impact events are assessed in the form of absolute error, the mean residual displacement error is calculated to be 2.1 mm (0.08 in.), with a standard deviation of approximately 1.7 mm (0.07 in.). This level of error is certainly appreciable; however, in the overall context of the problem, it is perhaps not of significant concern.

Although, in nearly all cases, the slab impact analysis procedure was found to remain stable throughout the performance of the multiple consecutive impact analyses, the accuracy of the computed responses were found to deteriorate over the progression of the impact protocols. This reduction was particularly evident in the analyses of the later impact events pertaining to the R/FRC slabs. In the case of slab R/FRC slab TH5, the ninth and tenth impacts performed on the slab were omitted due to the development of numerical instability. In Figure 11, computed-to-experimental ratios for the peak center-point displacements, peak support reaction forces, and the peak impulses are plotted over the progression of impacts (i.e., impact event numbers). From the figure, it can be seen that the peak displacements and the peak reaction forces were computed with reduced accuracies in the later impact events when compared to the results from the initial events. However, the computed impulses were shown to provide reasonable agreement with the experimental data throughout the full progression of analyses.

Note that some level of error accumulation should be anticipated when performing consecutive finite element analyses which rely on the progressive development of material damage. However, this form of error accumulation is likely only partially responsible for the differences obtained between the computed and measured responses for the later impact event R/FRC slab analyses.

Further, it should also be noted that all analyses of the R/FRC slabs were performed considering a simple back-bone monotonic steel fiber-tension constitutive response, computed on the basis of the Simplified Diverse Embedment Model (SDEM). As such, plastic strains resulting from local fiber slip and fiber pullout at crack locations have been neglected. Extending the current monotonic fiber-tension model such that plastic strain offsets can be incorporated within the material modeling of SFRC subjected to load reversals could potentially address some of the deficiencies encountered in the analyses of the R/FRC slabs.

SUMMARY AND CONCLUSIONS

The suitability of a layered thick-shell nonlinear finite element analysis procedure for the modeling and assessment of RC and R/FRC slab-like elements under repeated high-mass low-velocity impact loading conditions was investigated. Experimental data reported in the literature were used for verification and the merits and limitations of the computed slab response estimates developed were appraised by way of their accuracy in capturing slab center-point displacement responses, slab support reaction and impulse responses, slab displaced shapes, and slab steel reinforcing bar strain-time histories.

The work presented in this paper supports the following conclusions:

- In combination with the DSFM concrete material modeling, the layered thick-shell finite elements comprising the nonlinear analysis program were capable of providing reliable assessments for RC and R/FRC elements under impact. Using basic modeling techniques and simple finite element meshes, high accuracy estimates were obtained for the center-point displacement-time histories and the displaced shapes of the slabs comprising the experimental program.
- The punching shear failure modes which governed the behaviors of RC slab TH2 and R/FRC slab TH4, and nearly all others, were captured well in the numerical analyses.
- Peak support reaction forces were estimated with less, but still acceptable, accuracy. The general shapes of the reaction force-time histories and the support reaction impulse-time histories computed for the slabs were in good agreement with those measured experimentally.
- The computed post-peak vibrations of the slabs provided reasonable estimates of the experimental response frequencies. However, discrepancies existed between the numerical and the experimental post-peak damping characteristics, with the numerical results having the tendency to underestimate apparent damping.
- The nonlinear analysis procedure proved to be capable of performing sequential impact analyses on damaged specimens. In general, analyses of the RC slabs remained stable throughout the multiple event impact loading protocols. Instabilities were observed in the later-event analyses for some of the R/FRC slabs (e.g., R/FRC slab TH5).
- Lastly, the use of minimal stiffness proportional damping assignments were effective in stabilizing the analyses. The constant stiffness proportional damping assignments that were used for all specimens and all impact events in this study should be viewed as a practical approach for assigning supplemental damping.

REFERENCES

ACI Committee 318, “Building Code Requirements for Structural Concrete (ACI 318-14) and Commentary,” American Concrete Institute, Farmington Hills, MI, 2014.

Bentz, E.C. (2000). “Sectional Analysis of Reinforced Concrete Members”, Ph.D. Dissertation, University of Toronto, Department of Civil Engineering, 316 pp.

CEB-FIP (1988). “Concrete Structures under Impact and Impulsive Loading – Synthesis Report”, Comité EURO-International du Béton, Bulletin D’Information, No. 184, 184 pp.

Chen, Y. and May, I.M. (2009). “Reinforced concrete members under drop weight impacts”, Proceedings of the Institution of Civil Engineers, Structures and Buildings, No. 162, Issue SB1, February 2009, pp. 45-56.

El-Dakhakhni, W.W., Changiz Rezaei, W.F., Mekky, W.F., and Razaqpur, A.G. (2009). “Response sensitivity of blast-loaded reinforced concrete structures to the number of degrees of freedom”, *Canadian Journal of Civil Engineering*, Vol. 36, No. 8, August 2009, pp. 1305-1320.

fib Model Code (2010). Final Draft, Volume 1, International Federation for Structural Concrete, Bulletin No. 65, Lausanne, Switzerland, March 2012, 350 pp.

Figueiras, J.A. and Owen, D.R.J. (1984). “Analysis of Elasto-Plastic and Geometrically Nonlinear Anisotropic Plates and Shells” in Hinton, E. and Owen, D.R.J. (1984). “Finite Element Software for Plates and Shells”, Pineridge Press Limited, Swansea, U.K., 1984, 403 pp.

Guner, S. (2008). "Performance Assessment of Shear-Critical Reinforced Concrete Plane Frames", Ph.D. Dissertation, University of Toronto, Department of Civil Engineering, 429 pp.

Guner, S. and Vecchio, F.J. (2012). "Simplified Method for Nonlinear Dynamic Analysis of Shear-Critical Frames", *ACI Structural Journal*, Vol. 109, No. 5, September-October 2012, pp. 727-738.

Hrynyk, T. D. (2013). "Behaviour and modelling of reinforced concrete slabs and shells under static and dynamic loads." Ph.D. Dissertation, Dept. of Civil Engineering, Univ. of Toronto, Toronto.

Hrynyk, T.D., Vecchio, F.J. (2014). "Behavior of Steel Fiber-Reinforced Concrete Slabs under Impact Load", ACI *Structural Journal*, Vol. 111, No. 5, Sep-Oct, pp 1213-1224.

Hrynyk, T.D. and Vecchio, F.J. (2015). "Capturing Out-of-Plane Shear Failures in the Analysis of Reinforced Concrete Shells", ASCE Journal of Structural Engineering, April 2015, DOI: 10.1061/ (ASCE) ST.1943-541X.0001311.

Hrynyk, T.D. and Vecchio, F.J. (2016). "Modeling of Steel-Concrete Composite Elements under In-Plane and Out-of-Plane Loads", ASCE Journal of Structural Engineering, DOI: 10.1061/ (ASCE) ST.1943-541X.0001554.

Johansen, K.W., Brudlinieteorier, Jul. Gjellerups Forlag, Copenhagen, 1943, 191 pp. (Yield-line Theory, Translated by Cement and Concrete Association, London, 1962, 181 pp.)

Kennedy, R.P. (1976). "A review of procedures for the analysis and design of concrete structures to resist missile impact effects", *Nuclear Engineering and Design*, Vol. 37, No. 2, May 1976, pp. 183-203.

Kishi, N., Mikami, H., Matsuoka, K.G., and Ando, T. (2002). "Impact behavior of shear-failure-type RC beams without shear rebar", *International Journal of Impact Engineering*, Vol. 27, No. 9, October 2002, pp. 955-968.

Lee, S.C., Cho, J.Y. and Vecchio, F.J. (2013). "Simplified Diverse Embedment Model for Steel Fiber-Reinforced Concrete Elements in Tension", ACI *Materials Journal*, Vol. 110, No. 4, Jul-Aug 2013, pp. 403-412.

Lee, S.C., Cho, J.Y. and Vecchio, F.J. (2016). "Analysis of Steel Fiber-Reinforced Concrete Elements Subjected to Shear", ACI *Structural Journal*, Vol. 113, No. 2, Mar-Apr 2016, pp. 275-285.

LS-DYNA, Livermore Software Technology Corporation, Livermore, C.A., U.S.A.

Malvar, L.J. and Crawford, J.E. (1998). "Dynamic Increase Factors for Steel Reinforcing Bars", Proceedings of the Twenty-Eighth DoD Explosives Safety Seminar, Orlando, Florida, U.S.A., August 1998, 17 pp.

Mindlin, R.D. (1951). "Influence of rotary inertia and shear on flexural motions of isotropic, elastic plates", ASME *Journal of Applied Mechanics*, Vol. 18, No. 1, March 1951, pp. 31-38.

Newmark, N.M. (1959). "A Method of Computation for Structural Dynamics", ASCE *Journal of the Engineering Mechanics Division*, Vol. 85, 1959, pp. 67-94.

Polak, M.A. and Vecchio, F.J. (1993b). "Nonlinear Analysis of Reinforced-Concrete Shells", ASCE, *Journal of Structural Engineering*, Vol. 119, No. 12, December 1993, pp. 3439-3461.

Sliter, G.E. (1980). "Assessment of Empirical Concrete Impact Formulas", *Journal of the Structural Division*, Vol. 106, No. 5, May 1980, pp. 1023-1045.

UFC 3-340-02 (2008). "Structures to Resist the Effects of Accidental Explosions", Unified Facilities Criteria, U.S. Army Corps of Engineers, 2008, 1943 pp.

Vecchio, F.J. and Collins, M.P. (1986). "The Modified Compression Field Theory for Reinforced Concrete Elements Subjected to Shear", *ACI Structural Journal*, Vol. 83, No. 6, Nov-Dec, pp. 925-933.

Vecchio, F.J. (2000). "Disturbed Stress Field Model for Reinforced Concrete: Formulation", ASCE *Journal of Structural Engineering*, Vol. 126, No. 9, September 2000, pp. 1070-1077.

Wong, P., Vecchio, F. J., and Trommels, H. (2013). *VecTor2 and formworks manual*, 2nd Ed., Univ. of Toronto, Toronto, 347.

TABLES

Table 1 – Material Models and Analysis Options

Concrete Models		
Compression Base Curve	:	Popovics High Strength Concrete [1]
Compression Post-Peak	:	Modified Park-Kent
Compression Softening	:	Vecchio 1992-A [1]
Tension Stiffening	:	Modified Bentz [1]
Tension Softening	:	Linear
FRC Post-Crack Tension	:	SDEM
Confined Strength	:	Kupfer / Richart
Dilatation	:	Variable - Kupfer
Cracking Criterion	:	Mohr-Coulomb (stress)
Crack Stress Calculation	:	Basic (DSFM/MCFT) [1]
Crack Width Check	:	Crack Limit (agg/2.5)
Crack Slip Calculation	:	Walraven [1]
Hysteretic Response	:	Nonlinear w/ Plastic Offsets

[1] inherent to the formulations of the DSFM

Note: additional details provided in Wong et al. (2013)

Reinforcement Models		
Hysteretic Response	:	Elastic-Hardening (curvilinear)
Dowel Action	:	Tassios (crack slip)

Analysis Options		
Shear Analysis Mode	:	Parabolic Shear Strain
Strain History	:	Considered
Strain Rate Effects	:	CEB / Malvar-Crawford [2]
Structural Damping	:	Rayleigh [2]
Time Stepping Integration	:	Newmark - Constant Average [2]
Geometric Nonlinearity	:	Considered
Crack Allocation	:	Uniform: CEB-FIP 1978

[2] default dynamic analysis options

Table 2 – Summary of Center-Point Displacement Results for RC Slabs

		Peak Displacement			**Residual Displacement**			
Event	Impact Mass kg (lb)	Exp. mm (in.)	Comp. mm (in.)	Exp. / Comp.	Exp. mm (in.)	Comp. mm (in.)	Exp. / Comp.	| error | mm (in.)
TH2-1	150 (331)	13.2 (0.52)	14.0 (0.55)	1.06	2.7 (0.11)	0.3 (0.01)	0.12	2.4 (0.10)
TH2-2	180 (397)	18.7 (0.74)	21.5 (0.85)	1.15	3.0 (0.12)	2.2 (0.09)	0.71	0.9 (0.03)
TH2-3	210 (463)	26.6 (1.05)	29.1 (1.15)	1.10	8.9 (0.35)	9.6 (0.38)	1.08	0.7 (0.03)
TH6-1	150 (331)	18.3 (0.72)	17.2 (0.68)	0.94	6.2 (0.24)	1.7 (0.07)	0.28	4.5 (0.17)
TH6-2	180 (397)	27.7 (1.09)	29.6 (1.17)	1.07	11.4 (0.45)	10.3 (0.41)	0.90	1.1 (0.04)
TH7-1	150 (331)	12.8 (0.50)	13.1 (0.52)	1.02	2.6 (0.10)	0.3 (0.01)	0.12	2.3 (0.09)
TH7-2	180 (397)	18.3 (0.72)	18.5 (0.73)	1.01	3.3 (0.13)	0.9 (0.04)	0.28	2.3 (0.09)
TH7-3	210 (463)	28.5 (1.12)	23.7 (0.93)	0.83	11.5 (0.45)	5.7 (0.22)	0.49	5.8 (0.23)
			Mean =	1.02		Mean =	0.50	2.5 (0.10)
			C.O.V. =	9.1 %		C.O.V. [σ_{res}^{*}] =	68 %	[1.7 (0.07)]

Notes: Exp. = Experiment; Comp. = Computed; C.O.V. = coefficient of variation

* standard deviation of absolute residual displacement error

Table 3 – Summary of Center-Point Displacement Results for R/FRC Slabs

Event	Impact Mass kg (lb)	Peak Displacement			Residual Displacement			
		Exp. mm (in.)	Comp. mm (in.)	Exp. / Comp.	Exp. mm (in.)	Comp. mm (in.)	Exp. / Comp.	| error | mm (in.)
TH3-1	150 (331)	-	14.4 (0.57)	-	2.9 (0.11)	0.3 (0.01)	0.11	2.6 (0.10)
TH3-2	180 (397)	17.3 (0.68)	17.8 (0.70)	1.03	1.0 (0.04)	0 (0)	0.03	1.0 (0.04)
TH3-3	210 (463)	22.0 (0.87)	21.7 (0.85)	0.98	3.3 (0.13)	1.8 (0.07)	0.54	1.5 (0.06)
TH3-4	210 (463)	27.3 (1.07)	26.8 (1.06)	0.98	7.1 (0.28)	3.8 (0.15)	0.54	3.3 (0.13)
TH3-5	240 (529)	32.5 (1.28)	30.8 (1.21)	0.95	13.3 (0.52)	6.1 (0.24)	0.46	7.2 (0.28)
TH4-1	150 (331)	14.0 (0.55)	13.3 (0.52)	0.95	2.7 (0.11)	0.2 (0.01)	0.09	2.5 (0.10)
TH4-2	180 (397)	17.0 (0.67)	16.3 (0.64)	0.96	1.0 (0.04)	0.1 (0)	0.10	0.9 (0.04)
TH4-3	210 (463)	21.6 (0.85)	20.5 (0.81)	0.95	2.2 (0.09)	1.4 (0.06)	0.65	0.8 (0.03)
TH4-4	240 (529)	24.1 (0.95)	25.2 (0.99)	1.04	3.7 (0.15)	3.0 (0.12)	0.81	0.7 (0.03)
TH4-5	240 (529)	25.9 (1.02)	27.2 (1.07)	1.05	4.6 (0.18)	3.1 (0.12)	0.67	1.5 (0.06)
TH4-6	270 (595)	29.2 (1.15)	32.6 (1.28)	1.12	6.9 (0.27)	6.3 (0.25)	0.91	0.6 (0.02)
TH4-7	270 (595)	32.0 (1.26)	33.7 (1.33)	1.05	9.1 (0.36)	5.3 (0.21)	0.59	3.8 (0.15)
TH5-1	150 (331)	12.4 (0.49)	13.6 (0.54)	1.10	3.4 (0.13)	0.3 (0.01)	0.08	3.1 (0.12)
TH5-2	180 (397)	15.2 (0.60)	16.8 (0.66)	1.11	0.6 (0.02)	0 (0)	0.02	0.6 (0.02)
TH5-3	210 (463)	19.3 (0.76)	20.0 (0.79)	1.03	1.7 (0.07)	1.4 (0.06)	0.81	0.3 (0.01)
TH5-4	240 (529)	22.2 (0.87)	24.8 (0.98)	1.12	2.8 (0.11)	2.0 (0.08)	0.72	0.8 (0.03)
TH5-5	240 (529)	22.9 (0.90)	28.0 (1.10)	1.22	2.8 (0.11)	4.6 (0.18)	1.65	1.8 (0.07)
TH5-6	270 (595)	25.7 (1.01)	34.2 (1.35)	1.33	4.0 (0.16)	7.7 (0.30)	1.94	3.7 (0.15)
TH5-7	270 (595)	26.3 (1.04)	36.2 (1.43)	1.38	4.0 (0.16)	8.2 (0.32)	2.05	4.2 (0.17)
TH5-8	300 (661)	29.1 (1.15)	43.0 (1.69)	1.48	5.4 (0.21)	11.7 (0.46)	2.17	6.3 (0.25)
TH8-1	150 (331)	13.5 (0.53)	12.8 (0.50)	0.95	2.7 (0.11)	0.3 (0.01)	0.12	2.4 (0.09)
TH8-2	180 (397)	17.0 (0.67)	15.4 (0.61)	0.91	0.7 (0.03)	0.1 (0)	0.18	0.6 (0.02)
TH8-3	210 (463)	20.4 (0.80)	19.1 (0.75)	0.94	1.0 (0.04)	1.5 (0.06)	1.54	0.5 (0.02)
TH8-4	240 (529)	23.7 (0.93)	22.2 (0.87)	0.94	2.5 (0.10)	1.4 (0.06)	0.57	1.1 (0.04)
TH8-5	240 (529)	25.0 (0.98)	23.9 (0.94)	0.96	3.2 (0.13)	2.8 (0.11)	0.87	0.4 (0.02)
TH8-6	270 (595)	27.3 (1.07)	27.2 (1.07)	1.00	4.4 (0.17)	2.6 (0.10)	0.59	1.8 (0.07)
TH8-7	270 (595)	27.5 (1.08)	29.7 (1.17)	1.08	5.2 (0.20)	4.0 (0.16)	0.76	1.2 (0.05)
TH8-8	300 (661)	31.5 (1.24)	39.2 (1.54)	1.24	8.8 (0.35)	10.2 (0.4)	1.16	1.4 (0.06)
			Mean =	1.07		Mean =	0.74	2.0 (0.08)
			C.O.V. =	13 %		C.O.V. [σ_{res}^*] =	83 %	[1.7 (0.07)]

Notes: Exp. = Experiment; Comp. = Computed; C.O.V. = coefficient of variation
* standard deviation of absolute residual displacement error

FIGURES

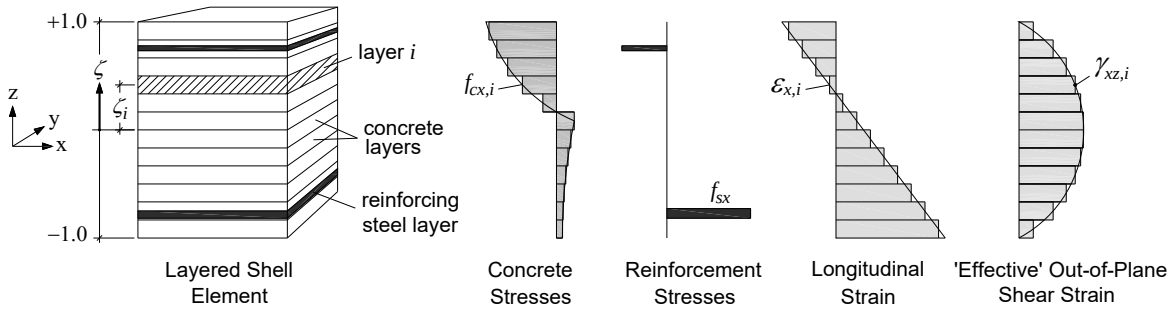

Figure 1 - Typical Sectional Response for the Layered 'Thick-Shell' Finite Element

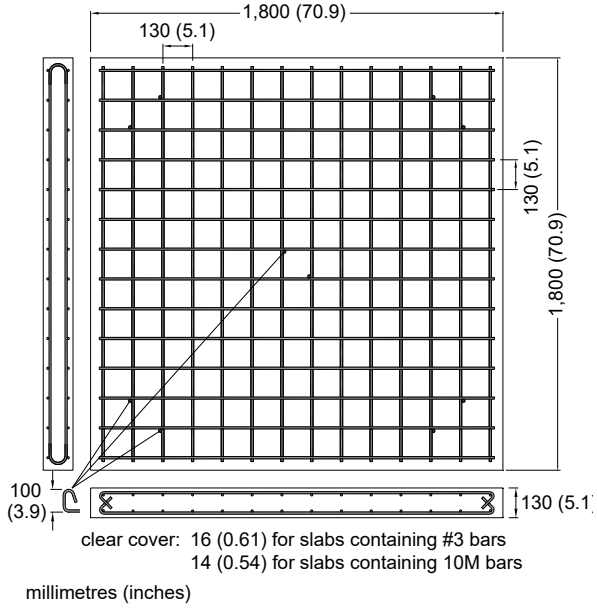

(a) Typical Slab Reinforcement Layout

Slab	Long. Reinf. Ratio ρ_l [1], %	Rebar / Spacing, mm (in.)	Fiber Volume Fraction V_f, %
TH2	0.420	#3 / 130 (5.1)	-
TH3	0.420	#3 / 130 (5.1)	0.50
TH4	0.420	#3 / 130 (5.1)	1.00
TH5	0.420	#3 / 130 (5.1)	1.50
TH6	0.273	#3 / 200 (7.9)	-
TH7	0.592	10M / 130 (5.1)	-
TH8	0.592	10M / 130 (5.1)	1.00

[1] based on total section height; per layer of steel

(b) Matrix of Test Specimens

RC Slab	Longitudinal Reinforcement Ratio ρ_l, %	Nominal Flexural Strength P_F [1], kN (kip)	Nominal Shear Strength P_V [1], kN (kip)	P_V / P_F
TH2	0.420	170 (38)	400 (90)	2.4
TH6	0.273	115 (26)	400 (90)	3.5
TH7	0.592	225 (51)	400 (90)	1.8

[1] notes: using f_c' = 50 MPa (7.3 ksi), f_y = 500 MPa (72.5 ksi)
concentrated loading area: 300 x 300 mm (11.8 x 11.8 in.)

(c) Estimated Static Capacities

Figure 2 – Details of Slab Specimens

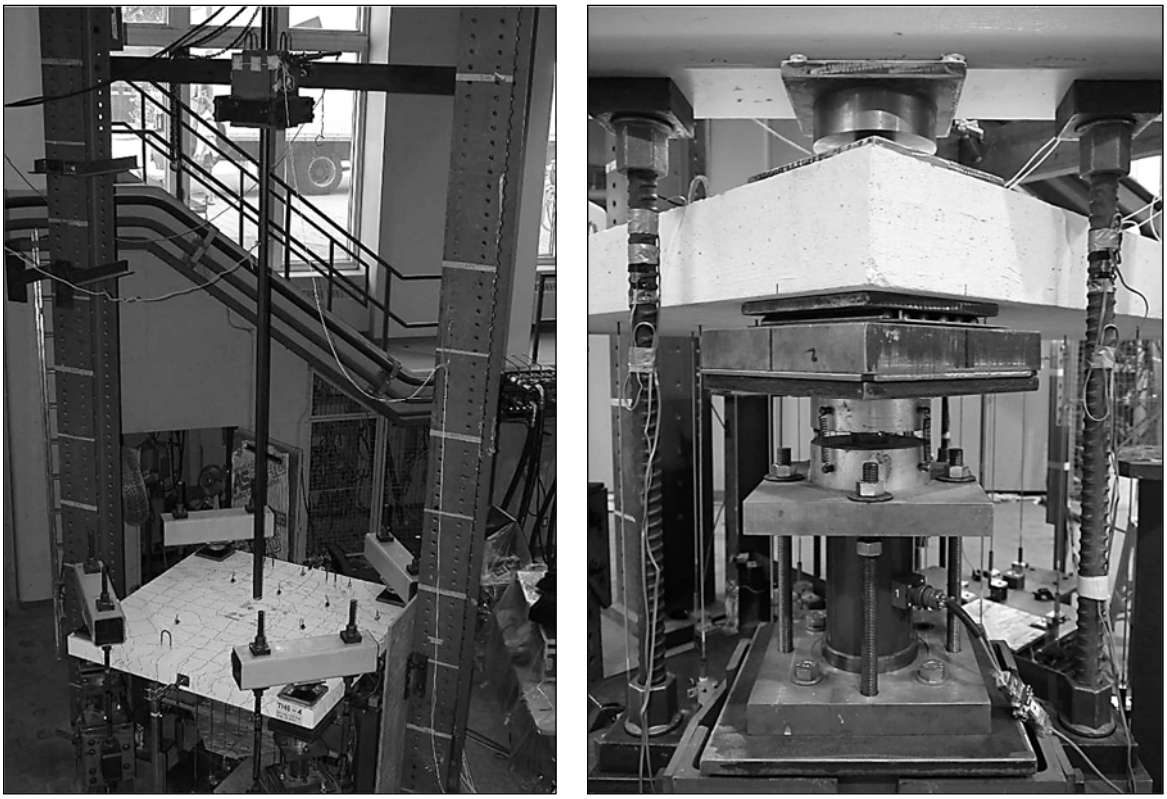

(a) Drop-Weight Test Frame (b) Corner Restraint Assembly

Figure 3 – Slab Impact Test Setup

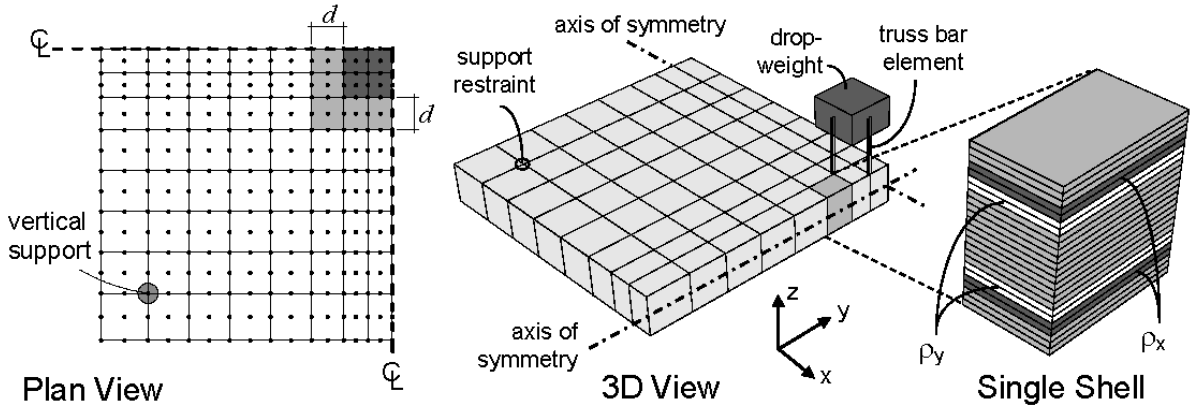

Figure 4 – Quarter-Slab Finite Element Model

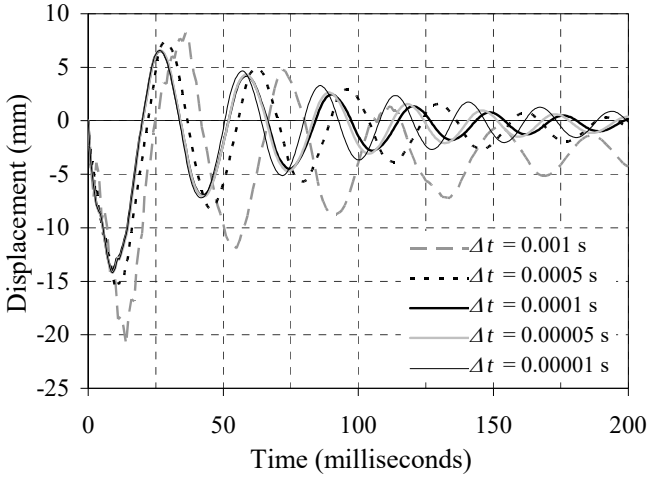

[Note: 1 in. = 25.4 mm]

Figure 5 – Influence of Δt on Computed Center-Point Displacement – Time Response; Event TH2-1

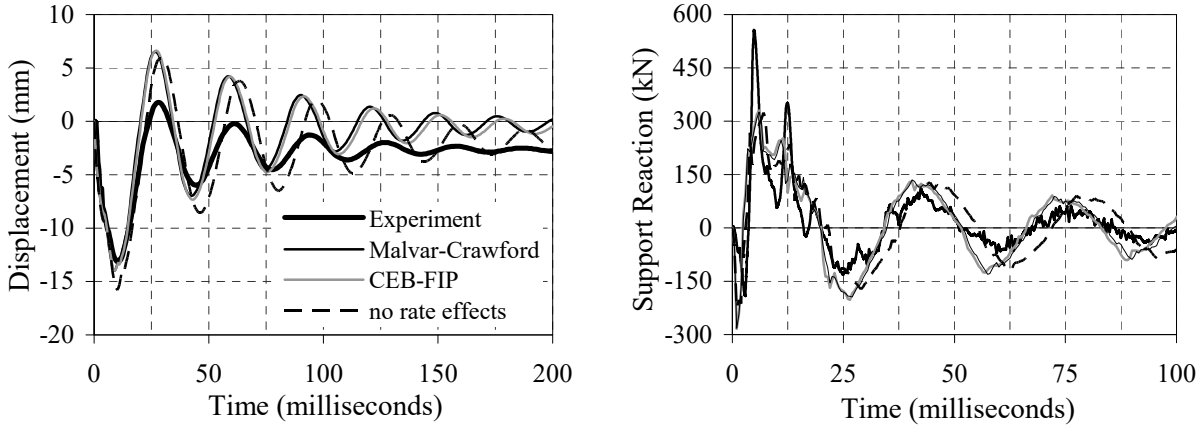

(a) center-point displacement-time history

(b) support reaction-time history

[Note: 1 in. = 25.4 mm; 1 kip = 4.448 kN]

Figure 6 – Influence of Strain Rate Effects on Computed Response - Time Histories; Impact Event TH2-1

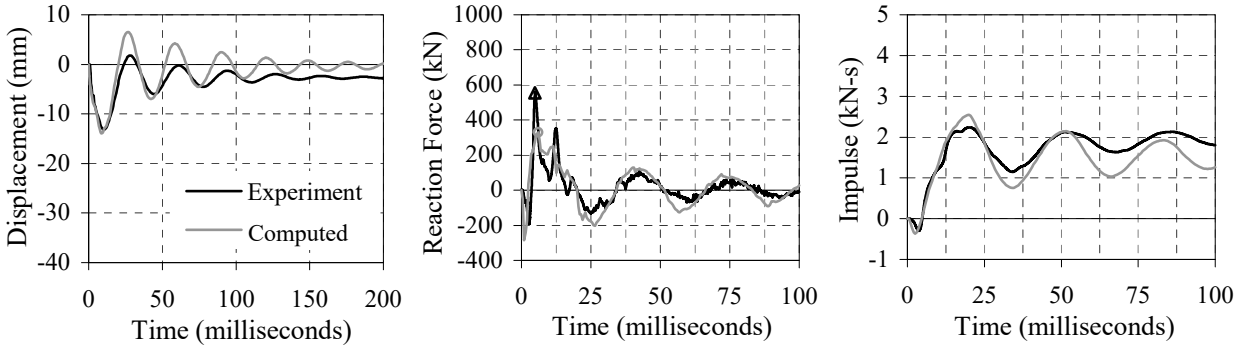

(a) Impact Test TH2-1 (first impact event, impact mass = 150 kg (331 lb))

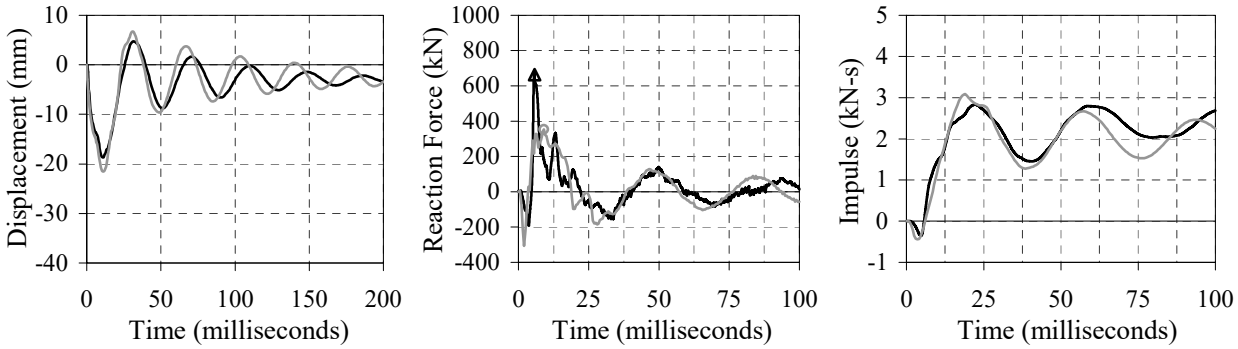

(b) Impact Test TH2-2 (second impact event, impact mass = 180 kg (397 lb))

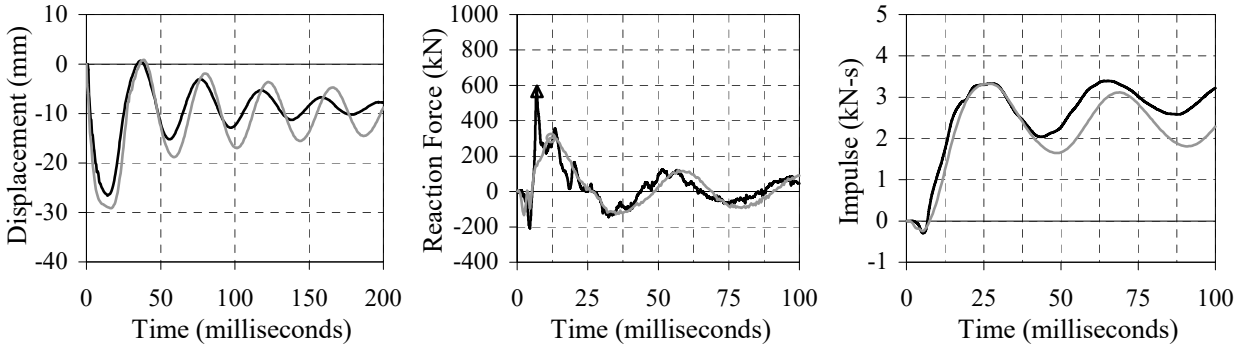

(c) Impact Test TH2-3 (third impact event, impact mass = 210 kg (463 lb))

[Note: 1 in. = 25.4 mm; 1 kip = 4.448 kN; 1 kip-s = 4.448 kN-s]

Figure 7 – Computed Response - Time Histories; RC Slab TH2 ($\rho_l = 0.420$ %; $V_f = 0$)

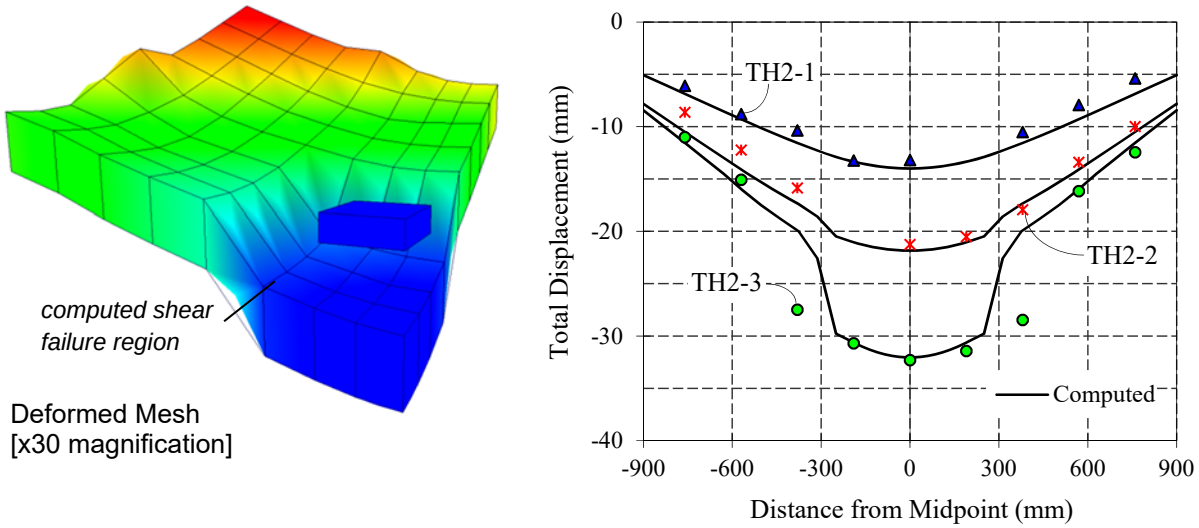

Figure 8 – Computed Displacement Profile; RC Slab TH2 ($\rho_l = 0.420$ %; $V_f = 0$) [Note: 1 in. = 25.4 mm]

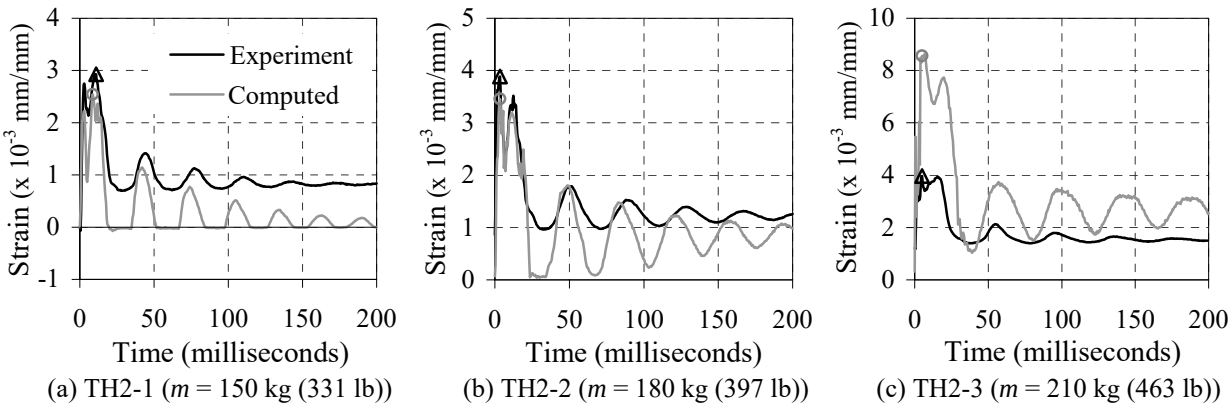

(a) TH2-1 (m = 150 kg (331 lb)) (b) TH2-2 (m = 180 kg (397 lb)) (c) TH2-3 (m = 210 kg (463 lb))

Figure 9 – Computed Reinforcing Bar Strain - Time Histories; RC Slab TH2 ($\rho_l = 0.420$ %; $V_f = 0$)

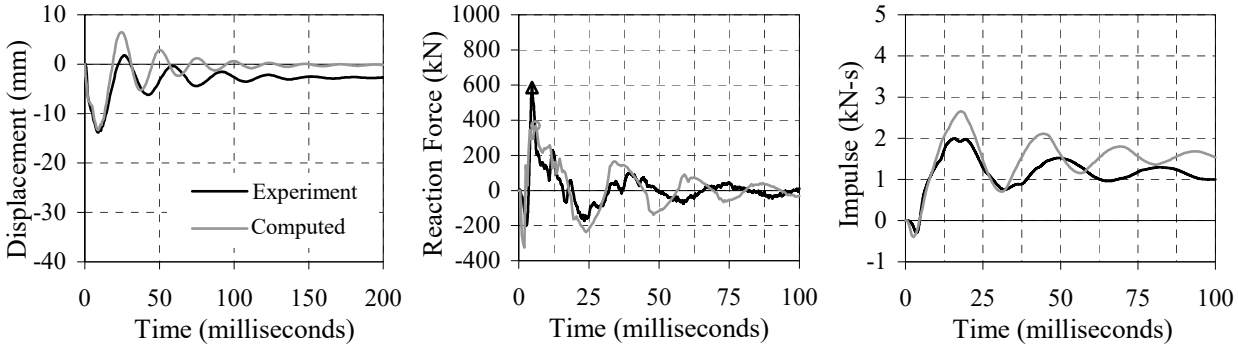

(a) Impact Test TH4-1 (first impact event, impact mass = 150 kg (331 lb))

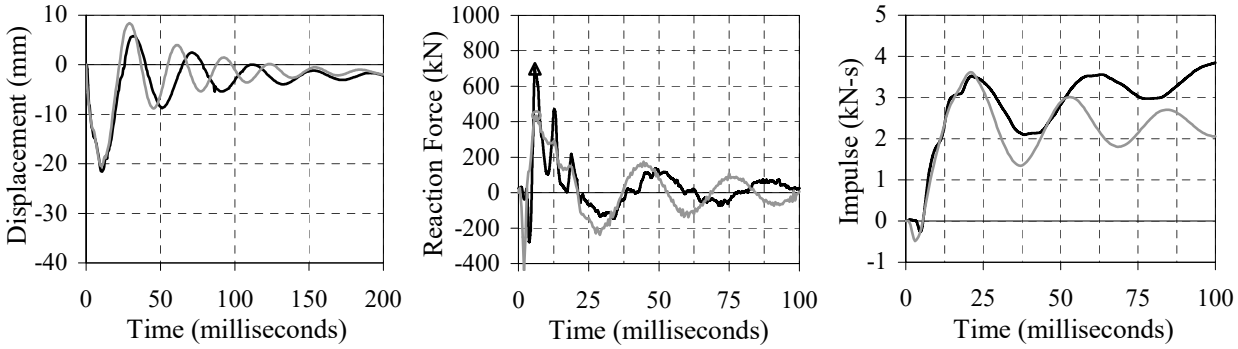

(b) Impact Test TH4-3 (third impact event, impact mass = 210 kg (463 lb))

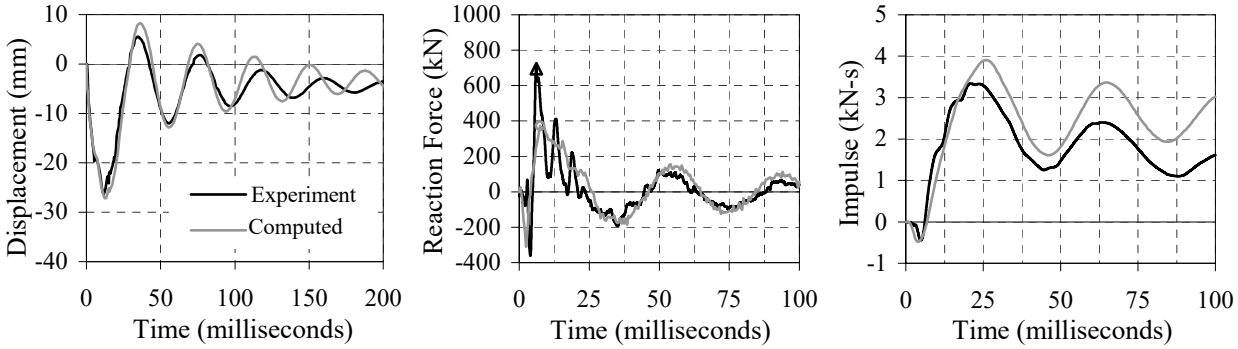

(e) Impact Test TH4-5 (fifth impact event, impact mass = 240 kg (529 lb))

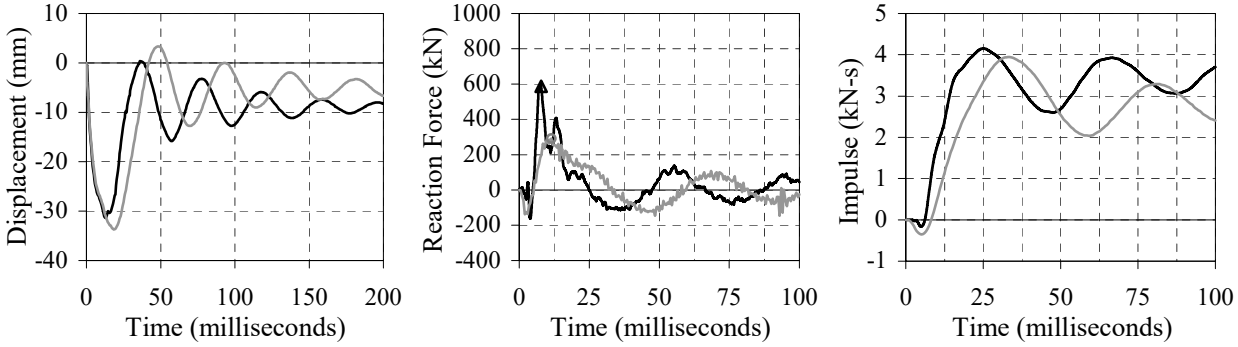

(g) Impact Test TH4-7 (seventh impact event, impact mass = 270 kg (595 lb))

[Note: 1 in. = 25.4 mm; 1 kip = 4.448 kN; 1 kip-s = 4.448 kN-s]

Figure 10 – Computed Response - Time Histories; R/FRC Slab TH4 (ρ_l = 0.420 %; V_f = 1.00 %)

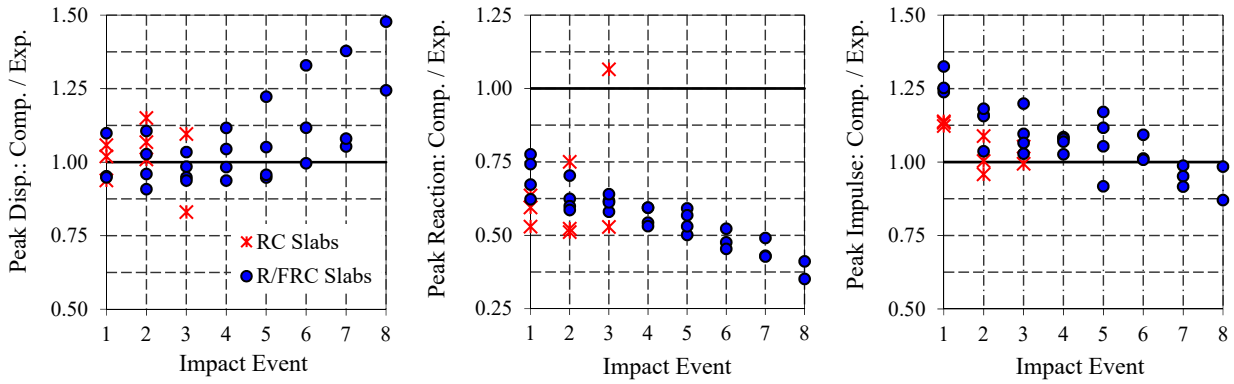

Figure 11 – Accuracy of Computed Results over Impact Progression